




Article

Prestressing Effect of Shape Memory Alloy Reinforcements under Serviceability Tensile Loads

Markus Beßling ^{1,*} , Christoph Czaderski ²  and Jeanette Orlowsky ¹ 

¹ Department of Building Materials, TU Dortmund University, 44227 Dortmund, Germany; jeanette.orldowsky@tu-dortmund.de

² Structural Engineering Research Laboratory, Empa, Swiss Federal Laboratories for Materials Sciences and Technology, 8600 Dübendorf, Switzerland; Christoph.Czaderski@empa.ch

* Correspondence: markus.bessling@tu-dortmund.de

Abstract: Repairing and strengthening of existing aged steel-reinforced concrete structures is a major challenge. Today, much of the repair work completed is insufficient and brittle. A promising new solution for repair and strengthening tasks is the use of iron-based shape memory alloy (Fe-SMA). The pre-strained Fe-SMA components enable the pre-stressing of existing building components due to the heat-triggered contraction of the steel. Thus, deflections can be reduced or even recovered. In addition, the cracking process can be adapted, and an improvement in the load, under which the first crack appears, is possible. In this paper, the effects of pre-stress generated by activated Fe-SMA rebars, which were centrally embedded inside of a concrete specimen, are shown. The objective of the study is to quantify the improvement in the loads of the first crack and show the influences of the pre-stressing on the load-bearing behavior and the cracking process. For this purpose, axial tensile tests were performed on concrete bars with height, width, and length of 50 mm, 70 mm, and 900 mm, respectively. These were compared to usual construction steel rebars, pre-strained but nonactivated Fe-SMA rebars, and activated Fe-SMA steel rebars. The evaluation of crack patterns and openings was done using digital image correlation (DIC). The pre-stressing of the concrete causes an increase in the first crack loads of more than 150%, which indicates a clear improvement in the state of serviceability limit.

Keywords: iron-based shape memory alloy; shape memory effect; pre-stress; tensile tests; textile reinforced concrete



Citation: Beßling, M.; Czaderski, C.; Orlowsky, J. Prestressing Effect of Shape Memory Alloy Reinforcements under Serviceability Tensile Loads. *Buildings* **2021**, *11*, 101. <https://doi.org/10.3390/buildings11030101>

Academic Editor: Rita Bento

Received: 13 January 2021

Accepted: 26 February 2021

Published: 6 March 2021

Publisher's Note: MDPI stays neutral with regard to jurisdictional claims in published maps and institutional affiliations.



Copyright: © 2021 by the authors. Licensee MDPI, Basel, Switzerland. This article is an open access article distributed under the terms and conditions of the Creative Commons Attribution (CC BY) license (<https://creativecommons.org/licenses/by/4.0/>).

1. Introduction

Due to the strong economic growth of the 1950s and 1960s, many of our current reinforced concrete building structures are over 40 years old and in need of repair. With regard to annual construction output in non-residential buildings, the effort required to maintain existing buildings already exceeds by far the effort required to create new buildings. This immense demand for repair, which is often related to an increase in the structural load, also applies to engineering structures, such as tunnels, underpasses, and parking structures. Unfortunately, the durability of repair and maintenance work is often limited. Besides cracks, delamination due to insufficient bond strength and corrosion of the reinforcements are the most frequent damages.

In view of these data and the increasing need for repairs, new repair concepts for improving the quality and service life of building structures are absolutely necessary. This demand is further intensified when considering the aspect of sustainability. Therefore, a need for research into suitable new repair methods exists.

A new repair method was recently introduced in the building industry in Switzerland. The new method consists of newly developed iron-based shape memory alloys (Fe-SMA) ribbed rebars. The rebars are embedded in a layer of shotcrete, which is attached to the old structure, and the rebars can be prestressed by heating to 150–200 °C. The pre-stress

is triggered by an internal change of the crystal structure and not by pulling as in the conventional pre-stressing technology. The main advantages are that the Fe-SMA bars do not need ducts nor anchorages and have no friction during pre-stressing. Iron-based shape memory alloys are much cheaper compared with nickel-titanium (NiTi), which is only used in research to strengthen concrete [1–6].

Due to the application of pre-stressing forces, the approach of using Fe-SMA to strengthen existing reinforced concrete components is very promising because crack loads can be increased and/or crack widths/changes can be minimized. However, no permanent solutions are currently available, especially for cracked reinforced concrete structures with time-dependent varying crack widths. The use of pre-stressed Fe-SMAs in combination with reinforced concrete could make a significant contribution towards solving this problem.

In this paper, the properties of repair mortars/concretes and iron-based shape memory alloy reinforcements are discussed first. In the second part, a comparison of construction steel rebars with Fe-SMA ribbed bars embedded in concrete is carried out by means of tensile tests. These tests are intended to show the effects of pre-stressing generated by shape memory alloys in structural repairs. The novelty of this work is the evaluation of the cracking process and the direct comparison of the crack opening curves using a pure tensile test. The axial tensile test approximates the repair layer in a strengthened component subjected to bending loads.

2. Materials and Research Idea

2.1. Repair Mortar/Repair Concrete

The European standard series EN 1504 regulates “products and systems for the protection and repair of concrete structures” [7]. Within this standard, EN 1504 Part 9 contains “general principles for the use of products and systems”, which includes principles and methods for concrete restoration, structural strengthening, and the preservation or restoration of steel passivity. The methods for the realization of these principles require the use of repair mortars (RM) or repair concretes (RC).

Cement-bound systems are most frequently used for this purpose. In addition to the main binder component cement, additives, such as limestone powder, fly ash and silica fume, admixtures, and aggregate, are also used. The aggregate is based on the grain structure of the cement-bound repair materials. Mortar and concrete are divided into two groups on the basis of the aggregate. Mortars have a maximum aggregate size of 4 mm, while concretes consist of an aggregate size above 4 mm. Due to the usually limited dimensions of the areas in need of repair and the requirement for a minimum layer thickness depending on the maximum grain size (based on a simplified calculation rule: minimum layer thickness equal to three times the maximum grain size diameter), mortars or concretes with aggregates up to 8 mm are predominantly used.

In contrast to new building structures, these repair materials must adhere well to the old concrete. The adhesion (adhesive strength, σ_{adh}) between old and new materials is one key factor determining the durability of the repair work. To ensure a durable bond, good substrate preparation, sufficient surface tensile strength, and consideration of weather conditions are necessary. Additionally, it is necessary to adapt the repair materials to the existing concrete [2]. This usually requires cement-bound materials with lower/adapted elastic modulus and higher tensile strengths. This can be achieved by adding polymer dispersions or modifying the grading curves [8,9]. For the repair of large horizontal as well as “overhead” structures, the use of sprayed concrete/sprayed mortar is often appropriate [10].

While the concrete carries the compressive loads, the reinforcement carries the tensile load. When taking over the tensile loads, cracks inside the repair materials are inevitable. Unfortunately, cracks with widths above 0.1 mm enable liquids to penetrate the material, which can limit the service life. A solution for this limitation could be the use of pre-stressed reinforcements [11] or the restriction of crack widths below 0.1 mm. Mineral systems, such

as mortars and concretes, with crack widths ≤ 0.1 mm are virtually impermeable due to their self-healing effects. The amount of penetrating moisture depends on the crack width, water pressure, crack roughness, and component thickness [12,13]. The use of conventional steel reinforcements in repair concretes generally causes crack widths above 0.1 mm and requires sufficient concrete cover for corrosion protection. The requirement of a sufficient concrete cover for corrosion protection can be eliminated with reinforcements made of fiber-reinforced polymers [14].

An interesting new material for repair tasks is textile-reinforced concrete (TRC). In this composite material, technical textiles made of carbon or AR (alkali-resistant) glass, embedded in fine-grained concrete, carry the tensile loads. With mechanical properties comparable to those of steel-reinforced concrete, TRC has the following advantages: thin-walled structures, resource-saving, higher durability, and the potential for very finely distributed crack development (crack widths ≤ 0.1 mm and crack spacing ≤ 10 mm) in the building material. These characteristics can be achieved via the size and yarn structure of the textile mesh [10]. The foundations for the use of technical textiles in cement-bound materials were developed in the Collaborative Research Centers 528 and 532, financed by the DFG (German Research Foundation) [15].

Previous studies on repairs with textile concrete dealt with the strengthening of reinforced concrete members [16,17]. The regions in existing reinforced concrete members (e.g., floor slabs) that were subjected to tensile stresses were strengthened by applying layers of fine-grained concrete and technical textiles made of carbon fibers. The fine-grained concrete (maximum grain size 1 mm) was applied via spraying at low pressures. The high binder content resulted in a comparatively high flexural strength (>7 MPa) [17].

A new promising alternative is the use of Fe-SMA ribbed bars for pre-stressing the cementitious repair system [18,19]. Figure 1 illustrates this idea. The principal sketch shows a section of a reinforced concrete slab that is loaded uniformly with the load q . In order to increase the load-bearing capacity of the slab and/or to minimize the crack widths, strengthening of the slab is required (Figure 1a,b). The aim is to strengthen cracked, heavily stressed reinforced concrete components by means of a repair system based on embedded SMA rebars. The innovative repair system enables load increases (Δq), increases crack loads, and reduces existing crack widths/changes as well as existing component deflections (Δ_{defl}). In order to achieve this goal, a suitable repair system with Fe-SMAs must be developed. Therefore, the adhesive strength (σ_{adh}) and the activated pre-stressing force in particular (F_{prestr}) have to be analyzed.

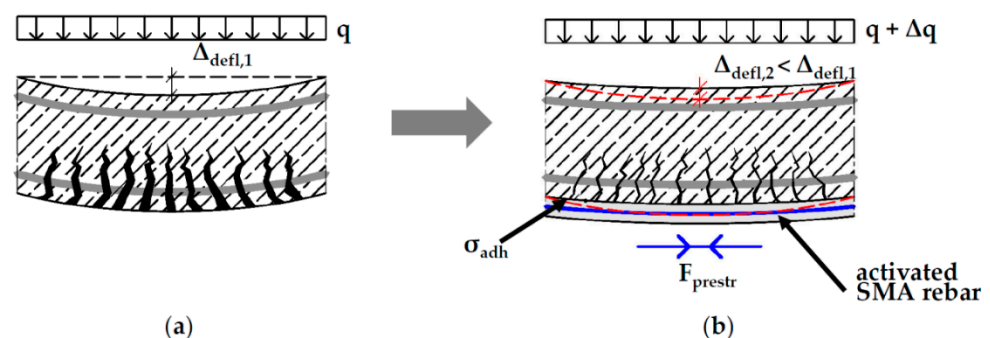


Figure 1. The principle idea of using iron-based shape memory alloy (Fe-SMA) for the repair and strengthening of existing steel-reinforced concrete structures; (a) before strengthening; (b) after strengthening with Fe-SMA embedded in an additional concrete layer.

2.2. Iron-Based Shape Memory Alloy (Fe-SMA)

SMAs belong to a group of “smart materials” that react automatically to changing environmental conditions. They have the property of returning to an initial shape upon heating—the so-called shape-memory effect (SME). Depending on the alloy, different properties such as superelasticity or the shape-memory effect can develop. The superelasticity

makes it possible to instantly revise deformations, e.g., due to earthquake loads [20]. However, for the shape-memory effect, the Fe-SMA needs to be pre-stretched (prestrained), and once the material has been installed, the SME is triggered by heating [18,21]. The SME is based on the different lattice structures (austenite and martensite), which are recoverable. These lattice structures can be changed by either mechanical stresses or temperature elevation [18].

For the application of Fe-SMAs in civil engineering, iron-based shape memory alloys (Fe-SMA) are most attractive due to their lower cost, higher elastic modulus, and relatively low activation temperature compared to NiTi (nickel titanium) or copper-based alloys [18]. The shape-memory effect in Fe-SMA is attributed to the stress-induced martensite transformation from the γ -austenite (fcc, face-centered-cubic) phase to the ε -martensite phase (hcp, hexagonal closed packed) at low and medium temperatures and the reverse transformation (ε to γ -phase) at high temperatures (≈ 100 – 250 °C) [22–24].

After production, the Fe-SMA bars are in the austenite phase state. Then, during pre-straining, the ε -martensite phases, which are recoverable, are produced. Then, after the Fe-SMA rebars are embedded in concrete and the concrete has fully cured, the rebars are heated via electric resistive heating or by simply heating the complete element as in this study (and cooling it down to room temperature), and the reverse transformation from martensite to austenite takes place. Therefore, because the shape recovery of the Fe-SMA rebars in the concrete is constrained, pre-stress is produced in the Fe-SMA rebars.

While at Empa, Swiss Federal Laboratories for Materials Science and Technology, Fe-SMAs based on Fe-Mn-Si-Cr-Ni-VC were developed [11,18,25,26], at the University in Kassel Fe-Mn-Al-Ni shape memory alloy was processed via additive manufacturing [27]. Adding small amounts of titanium to Fe-Mn-Al-Ni significantly enhances grain growth, which could allow a subsequent increase in preload forces in the future [28].

Up to now, the use of Fe-SMAs for strengthening reinforced concrete structures has been investigated intensively for many years at Empa, Switzerland [11,18,29]. The Fe-SMAs developed and patented at Empa are now being produced on an industrial scale [26]. The material is used for concrete reinforcement in two different variants:

- Pre-strained Fe-SMA plates, which are directly fixed by Hilti nails at their ends in the bending tension zone of the reinforced concrete components. The subsequent heating produces an external pre-stressed tension strip without any bond to the reinforced concrete [26,28]. With a pre-strain of 2% and after heating to 160 °C and cooling down to room temperature, an initial pre-stress of 300–350 MPa can be achieved [26,29].
- Pre-strained ribbed reinforcing rebars made of Fe-SMAs are applied in grooves in the bending tension zone of a reinforced concrete member. Afterwards the rebars are heated and the grooves are filled with cement-bound materials. Alternatively, the reinforcing bars can be connected to existing reinforced concrete components via an additional layer. In this variant, the pre-stressing element is bonded to the concrete [11,30] (Figure 2a). With a pre-stressing value of 4–6% and after heating to about 200 °C and cooling down to room temperature, an initial pre-stressing value of about 300 MPa can be achieved for a rebar with a diameter of 16 mm [11]. The achievable pre-stressing values are mainly controlled by the degree of pre-straining and the temperature [11].

Due to the possibility of activating the Fe-SMA rebars in different installation conditions, the pre-stressing influences can be controlled. By heating up the rebar while it is anchored solely on the ends of the existing structure, the activation forces are introduced in the existing component (see Figure 2a). The repair mortar applied afterwards is nearly free of tensile stresses. This results in a reduction in the resisting deflections and small cracks in low-crack distances in the repair layer by applying the loads after the repairing process [11,30]. In contrast to this, pre-stressing forces can also be introduced in the repair mortar via heat when the Fe-SMA rebar is embedded completely (see Figure 2b). Therefore, the first crack load of the repair layer will be higher. The option drawn in Figure 2b will be analyzed in the following experimental program.

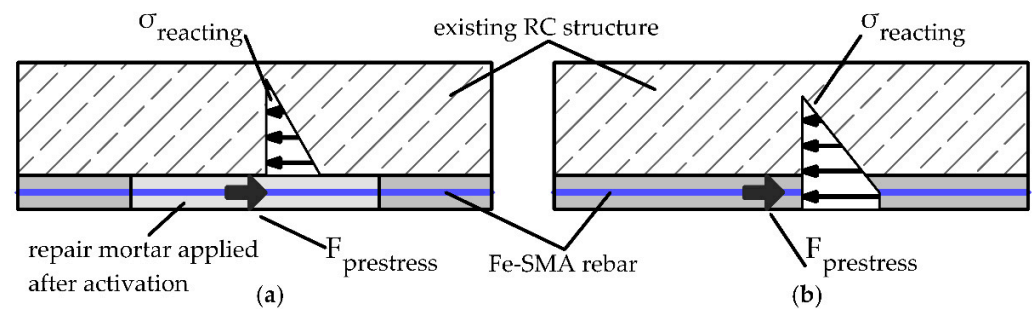


Figure 2. A schematic sketch of the influences of the installation conditions during the activation of the Fe-SMA rebar on the reacting tension (σ_{reacting}) in the existing repair concretes (RC) structure. (a) Fe-SMA rebar embedded only in the anchorage area and the application of heat in the free length afterwards; (b) Fe-SMA rebar embedded over the full length before applying heat.

3. Experimental Program

3.1. Aim of Investigation

The aim of this investigation is to show the composite behavior of the Fe-SMA ribbed bar compared to construction steel B500B by observing the development of the crack pattern and measuring the crack-opening force-curves. To compare the load-bearing behavior of the materials, a series of reinforced concrete axial tensile tests were performed. The repair layer of an RC beam under bending loads (Figure 1) was mainly subjected to tensile loading. Therefore, pure axial tensile tests were performed in order to investigate its stress and cracking behavior. To pre-stress the Fe-SMA rebars, the reinforced concrete specimens were heated to 160 °C in an oven (thermal treatment). Thereby, the increase in the first crack load due to the pre-stressing of the Fe-SMA rebars was also shown (Figure 2b). Consequently, the influence of the heating process on the concrete's properties was also investigated. The experimental study was divided into four steps. First, the characteristics of the concrete after 28 days were measured to test the workability and to check the concrete properties. In the next step, reinforced concrete tensile test samples (two with each material) were manufactured. After seven days of storage, two samples reinforced with Fe-SMA rebars were thermally treated to generate the pre-stressing in the rebars. Lastly, the tensile tests on the reinforced concrete tensile specimens were done.

3.2. Material Characterization

A fine-grained concrete with a maximum grain size of 8 mm and a large amount of binder was used. As a grading curve, the AB curve nearer to the fuller parabola was used. Fly ash was deliberately omitted due to its decreasing availability. The concrete was characterized by its high flowability and dense structure, which was reached by the composition of the filler and aggregates. It is a fine-grained concrete which can be classified as being between a normal concrete and a repair mortar. This ensures good bond performance and producibility of samples with small concrete covers. The concrete can also be used as a repair concrete. The ingredients of the concrete are listed in Table 1.

Table 1. Ingredients of the used concrete mix.

Component	Unit	Amount
Cement CEM I 42.5 R (c)		480
Water content (w)		205
Filler	kg/m ³	114
Sand 0–2 mm		652
Gravel 2–8 mm		864
Super-plasticizer	%/c	0.5
w/c-ratio	-	0.42

The hardened concrete properties were determined after 28 and 33 days. Tests were done according to EN 1015-11 [31] on samples of $40 \times 40 \times 160 \text{ mm}^3$ for compressive strength ($f_{c,m}$) and flexural strength ($f_{c,flx}$) as usual for mortars and fine-grained concretes. The samples were stored in the formwork for one day, underwater at $20 \text{ }^\circ\text{C}$ for six days, and subsequently at $20 \text{ }^\circ\text{C}$ and 65% relative humidity (r.h.). The 33d testing series included two sets of samples. While the first set was stored as mentioned before, the second set (33d-th) was thermally treated (see Section 3.3). Therefore, the influence of the thermal treatment on the hardened concrete's properties can be evaluated. Figure 3 shows the hardened concrete's properties after 28 and 33 days.

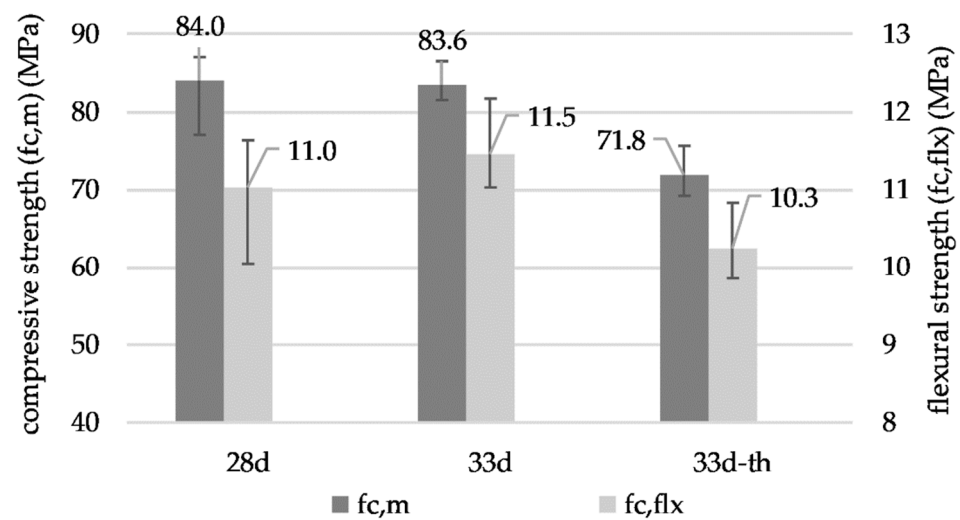


Figure 3. The hardened concrete's properties tested according to [31]. The mean values are shown (≥ 3 samples), the span is indicated, the series concerning the testing age is named (d), and the thermal treatment (th) is indicated.

The results point out that the thermal treatment reduces the concrete's performance by about 10%. The compressive strength as well as the flexural strength are lower. This reduction can be explained by the fast drying of the concrete due to the thermal treatment. The hydration process is reduced in parts of the specimen, and drying shrinkage also reduced the performance.

As a reinforcement, construction steel B500B and Fe-SMA rebars produced by the company re-fer AG [32] were used. The properties of the reinforcements necessary in this study are shown in Table 2. Further characteristics such as ultimate strain are presented elsewhere [11,33]. To enable a comparison, rebars with similar diameters were chosen. Hence, the percentages of reinforcement in the test specimens were also similar.

Table 2. The properties of the reinforcements.

Reinforcement	Unit	Construction Steel [34]	FE-SMA Rebar [32]	
			Prestrained Activated	Prestrained Nonactivated
Abbreviation	-	B500B	SMA	
Tensile strength	MPa	540	650	
Young's modulus	GPa	200	170–60	130–40
Diameter (mm)	mm	12	11	
Nominal cross section (A)	mm ²	113	105	
Percentage of reinforcement	%	3.2	3.0	

Figure 4 presents simplified stress-strain curves for the different types of reinforcements. The characteristic tensile loading behavior of the materials is visible. The construction steel (B500) shows linear elastic behavior up to its yield strength of 500 MPa. After reaching the yield stress, no considerable load increase is possible. The SMA steel has a varying Young's modulus which is about 170 GPa after pre-straining without activation and is reduced by increasing stresses in the material. In addition, the activated SMA steel rebar has different load-bearing behavior compared to the nonactivated one. It must be considered that the nonactivated SMA steel rebar is not applied in practice. Here, it is used as a reference to show the effects of pre-stressing in a direct way.

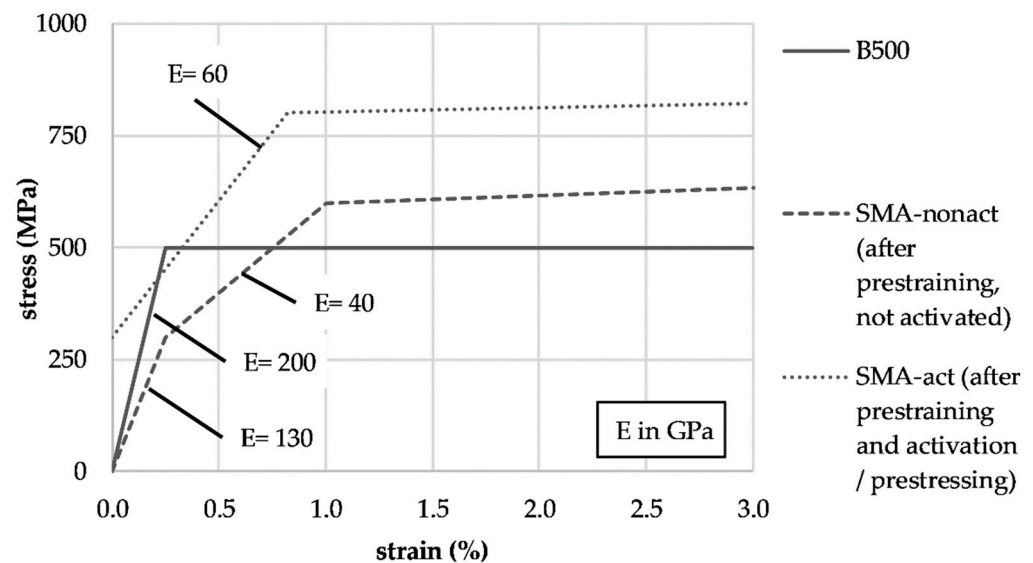


Figure 4. The simplified stress-strain curves for the different reinforcement types. B500: the calculation curve [34,35]; nonactivated Fe-SMA: linearized from [36]; activated Fe-SMA: linearization of a testing curve provided by re-fer AG.

3.3. Test Specimens and Experimental Setup

The reinforced concrete tensile test specimens had dimensions of 50 mm × 70 mm and a length of 900 mm. The specimens were reinforced with one rebar, which was placed centrally in the cross-section. In every wooden formwork, two specimens (of the same material) were produced. To ensure the position accuracy, the rebars were fixed at the ends of the formwork. Figure 5 shows the cross-sections of the specimens.

To activate pre-stressing in the Fe-SMA rebars, the specimens were heated to 160 °C. Therefore, two specimens were thermally treated in an oven. The specimens were heated until the core temperature of the specimen reached 160 °C. This temperature was held for 15 min. The core temperature was measured by a sensor in the middle of one specimen. Besides these specimens, for the characterization of the concrete's properties, one set of samples was also thermally treated to evaluate the influence of temperature on the concrete. The results are shown in Figure 3.

Uniaxial tensile tests were performed with the universal testing machine Inspect 100 from the company Hegewald und Peschke (Nossen, Germany). The forces were measured with a class 1 load cell with a maximum load of 50 kN with 50 Hz. The specimens were fixed into steel clamps and connected to the testing machine by a ball-bearing-mounted load introduction (Figure 6). As a consequence, a centric and free movable load introduction was possible. A DIC (digital image correlation) system ARAMIS 12M from the company GOM GmbH (Braunschweig, Germany) was used to measure the strains as well as the cracking process and crack pattern development. For this purpose, a stochastic black and white pattern was applied to the front of the specimens. The DIC measurement was done at a measuring rate of 1 Hz. The testing was displacement controlled at 1 mm/min, and all tests were stopped at 49 kN.

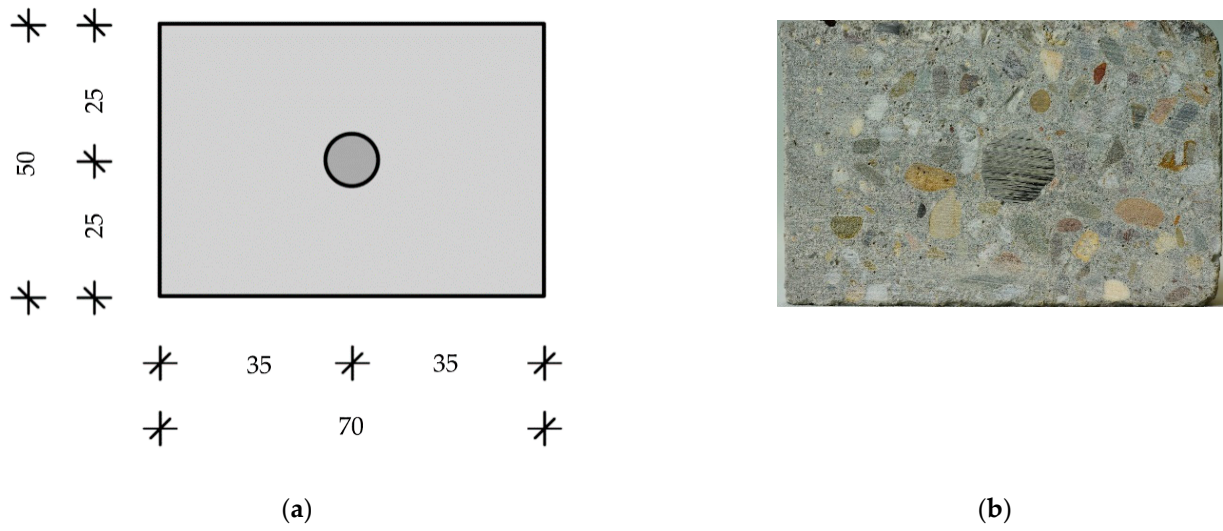


Figure 5. Specimen cross-sections: (a) schematic; (b) the cut-specimen after testing (anchorage area).

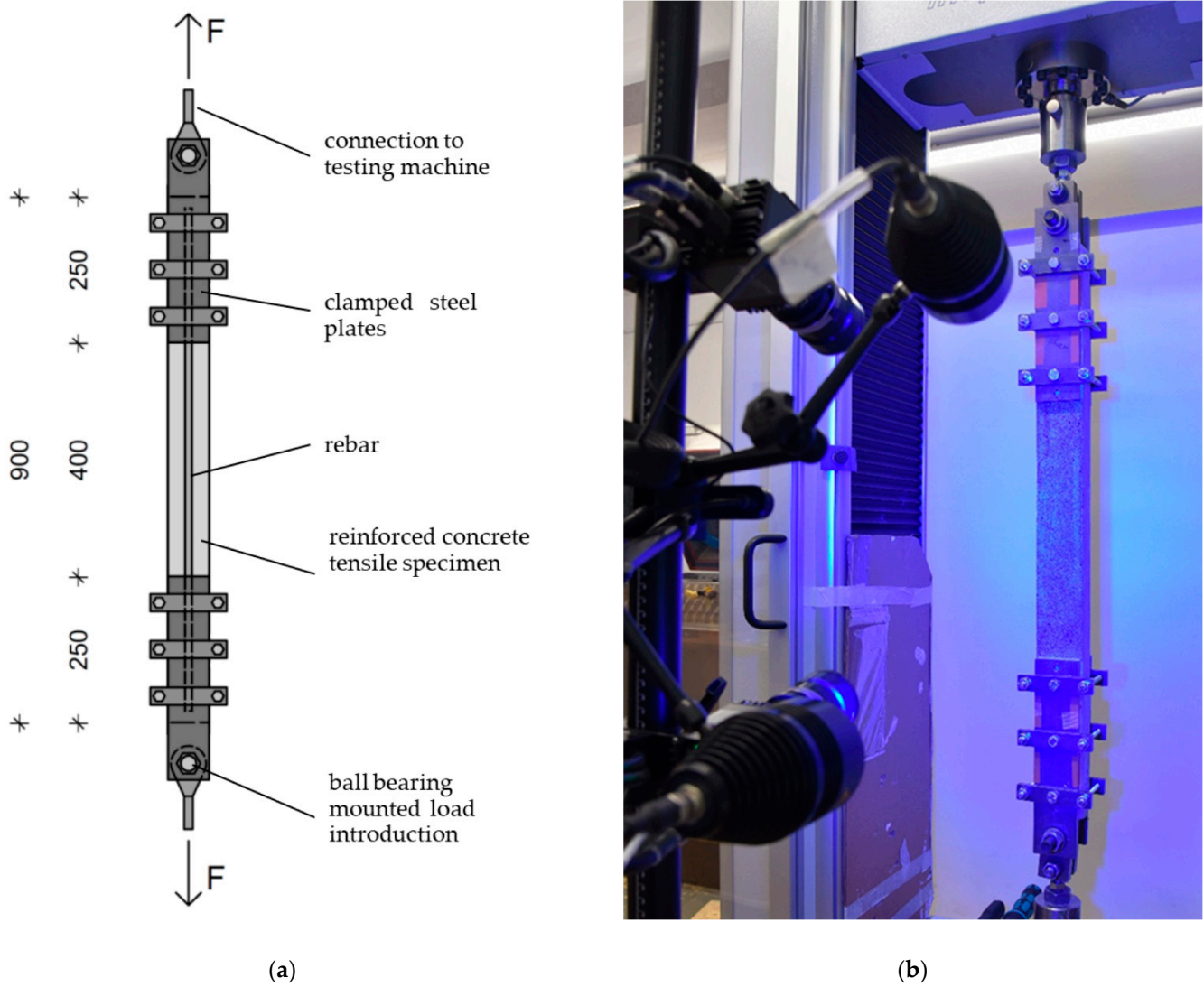


Figure 6. The test setup: (a) the schematic; (b) in the laboratory with the usage of digital image correlation (DIC).

4. Test Results

To give an overview of all tests, the force-machine displacement curves are shown in Figure 7. The results illustrate that both specimens of the same reinforcement type display similar load-bearing behavior. The differences between the two B500B curves can be explained by the failure of the load introduction in the first test. Therefore, for the following tests, the load introduction was enhanced. The differences between the different reinforcements can be observed in the first cracking load, the load decrease via cracking, and the curve progression. The B500 steel has the lowest first-crack load (8.6 kN), while the nonactivated Fe-SMA rebars had their first cracks at 12.0 kN. This difference can probably be explained by the fact that the positioning of the rebars in the specimen is not entirely centric. The high axial stiffness of the construction steel caused asymmetric loading. Therefore, cracks occurred on one side of the specimen and developed to the other side (Figure 9). This reduced the cracking loads and influenced the crack opening. By pre-stressing the Fe-SMA rebars, the first crack loads increased to 31.9 kN, which implies a growth of 166% compared to the nonactivated Fe-SMA rebars. The reduction in the concrete performance ($\approx 10\%$) due to thermal treatment would have a negligible effect on the first crack load; however, this was not notable due to the pre-stressed Fe-SMA rebars.

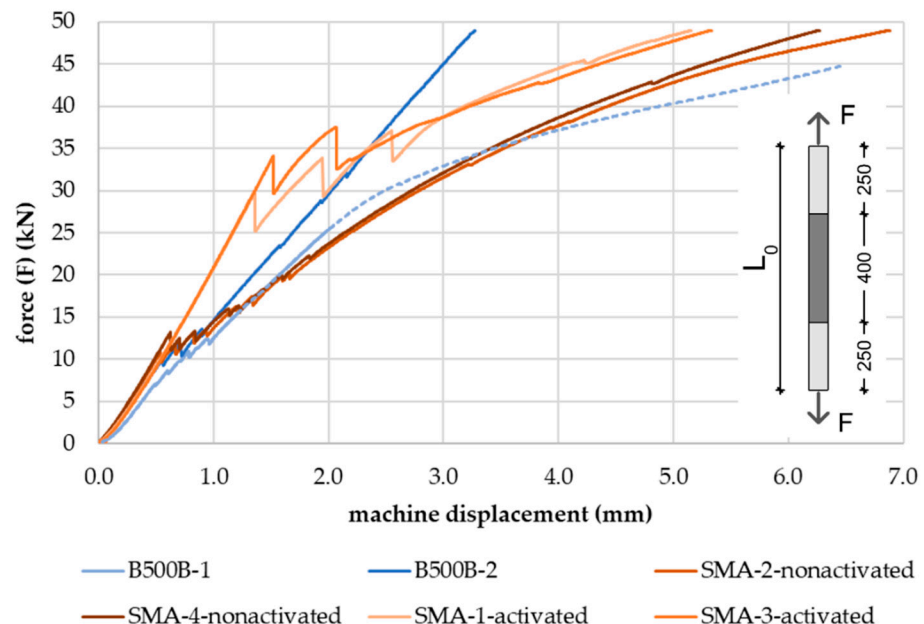


Figure 7. Force-machine displacement curves of the reinforced concrete tensile tests. Specimen age 32/33 d; testing speed: 1 mm/min; free length: $L_0 = 400$ mm; measuring rate: 50 Hz; naming: type of material, specimen number, nonactivated/activated (pre-stressed).

In Figure 8, the force-strain curves are presented. To measure the strain, the distance of the clamps measured by the DIC system was used. For readability, one exemplary specimen of each series is plotted. All curves show the typical three parts of a reinforced concrete structure under tensile load. After the first crack (part 1) occurred, the curve flattens due to cracking (part 2). After the cracking process is completed, the curve rises again. The first cracking load is mainly influenced by the concrete tensile strength and the pre-stressing of the rebar, as mentioned before. Parts 2 and 3 depend on the axial stiffness and the bonding performance of the reinforcement. Furthermore, the concrete's properties influence the cracking process. While the concrete properties of all specimens are similar, the EA's differ. Construction steel B500 exhibits a higher axial stiffness ($EA = 22,600$ GPa/mm²), which was also constant up to the end of the experiment. This is also visible in the comparably steep curve progression. After the cracking process, the curve is nearly linear. In the nonactivated Fe-SMA rebars, the reducing Young's modulus (Figure 4) with respect to the

increasing stresses can be seen in the concave curve progression. Regarding the SMA-1-th curve (pre-stressed), the serviceability of the composite material was clearly enhanced. The serviceability limit state can be set to about 20 kN, or about one-third (177 MPa) of the yield strength of construction steel. After the cracking process, the SMA-1-th curve proceeds nearly parallel to that of the nonactivated Fe-SMA rebars. This indicates that the activated Fe-SMA rebars behaved similarly to the nonactivated ones at higher loads when the effect of pre-stressing was overcome.

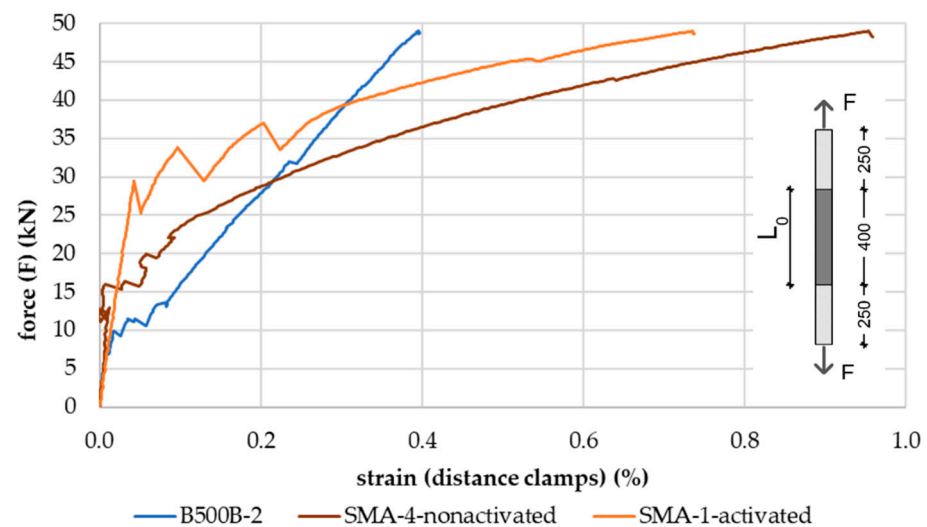


Figure 8. The force-strain curves of exemplary specimens of the reinforced concrete tensile tests. Specimen age 32/33 d; testing speed: 1 mm/min; free length (distance clamps): $L_0 = 400$ mm. Strains were measured via DIC at a rate of 1 Hz. Naming: type of material, specimen number, nonactivated/activated (pre-stressed).

The crack distribution as well as the development of the crack pattern were observed using a DIC measurement system. Figure 9 shows the specimen's surfaces with plotted strains at the loads of 20 kN and 40 kN. Under a load of 20 kN, the B500B (20 kN = 177 MPa) and the SMA (not thermally treated) contain most of the cracks and can be located in part 3 of the force-strain curve. Due to the axial stiffness of the rebars, some cracks developed from one side of the specimen to the other. In the case of the activated Fe-SMA rebars (SMA-1-th), no cracks are visible. Because of the pre-stress force of the Fe-SMA rebars, the specimen remained uncracked.

Considering the crack patterns at a load of 40 kN, the widening of the cracks in the case of the B500B and SMA (nonactivated) specimens can be observed. In addition, the pre-stressed specimen (SMA-1-th) shows cracks. B500 has the lowest crack spacings (≈ 5 cm), while the crack spacings of the SMA are about 7 cm wide. Due to the pre-stressed concrete, the distance between the cracks of the activated SMA steel are clearly larger (≈ 15 cm). Besides the typical tensile cracks, the beginning of longitudinal cracks along the rebar is visible. This can be explained by the low concrete cover of about 19 mm ($1.5 \times d_{\text{reinf.}}$).

For the comparison of the bonding performance of the materials, the force-crack-opening curves of the representative cracks are shown in Figure 10. The crack opening was measured with two digital extensometers (w_1 and w_2) of the DIC. The extensometers were placed near the specimen's edges. The mean value of both extensometers is plotted in Figure 10. Shown are two cracks located in the free measuring area that occurred in an early stage of the cracking process. They were chosen as exemplary cracks.

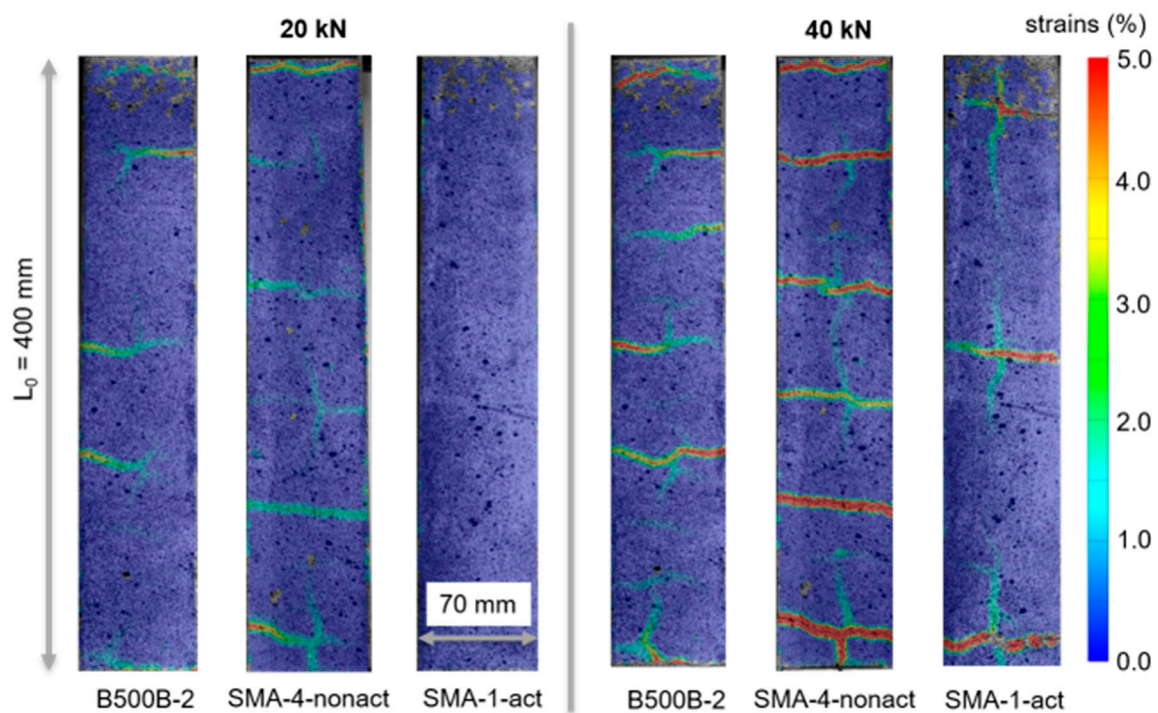


Figure 9. DIC pictures with marked strains and loads of 20 kN and 40 kN. Specimen age, 32/33 d; naming: type of material, specimen number, nonactivated/activated (pre-stressed).

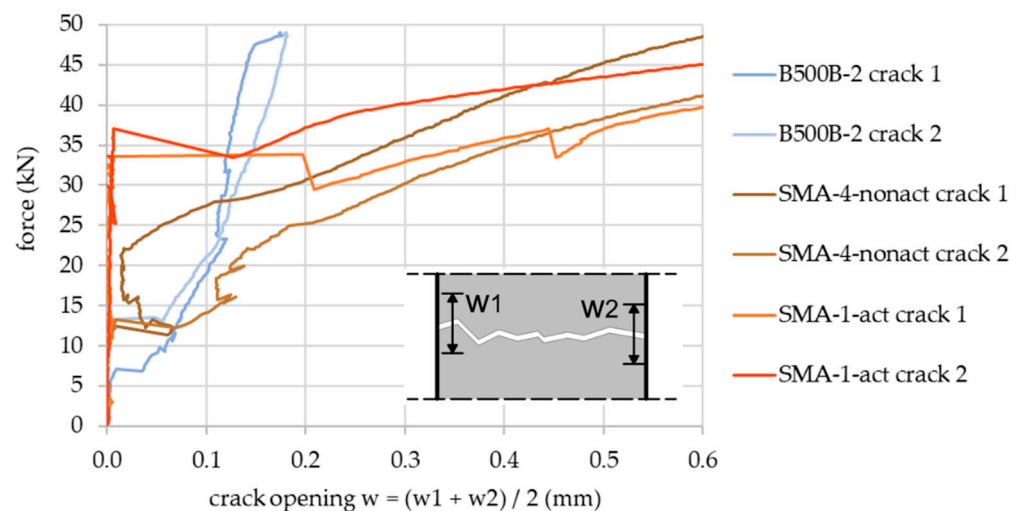


Figure 10. The force-crack-opening curves of the representative cracks. The crack opening is the mean value of two digital (DIC) extensometers. Naming: type of material, specimen number, nonactivated/activated (pre-stressed).

The opening of the crack is influenced by the following cracks. This can be seen in the decreasing trend of the crack openings in the curves. While the first openings of the B500 and Fe-SMA rebars are comparable, the following development differs. Due to the steeper ribs and greater EA of the construction steel compared to the SMA rebars, the force-crack-opening curves are clearly steeper. Both materials behaved similarly at the state of the serviceability limit. Here, the specimens with pre-stressed SMA steel are uncracked. After the first cracks appear, the curve develops in a relatively flat manner and approaches the curves of the nonactivated Fe-SMA rebars. These results underline the conclusion concerning the force-strain-curves (Figure 8) that the activated FE-SMA behave similarly to the nonactivated ones after the effect of pre-stressing is overcome.

5. Summary and Conclusions

For the evaluation of reinforced concrete material behavior under tensile loads, tensile tests were performed. Construction steel B500B rebars and Fe-SMA rebars were chosen as materials. A fine-grained concrete with a maximum grain size of 8 mm, a compressive strength of $f_{c,m,28d} = 84.0$ MPa, and a flexural strength of $f_{c,flx,28d} = 11.0$ MPa was used to produce the specimens. Fe-SMA rebar concrete composite specimens in the shape of 900 mm long concrete bars with a cross-section of 50 mm \times 70 mm were tested, both in their nonactivated and activated (pre-stressed) states, to consider the effects of the pre-stressing in a direct way. In both cases, the Fe-SMA rebars were pre-strained. For each material (B500B, nonactivated Fe-SMA, activated/pre-stressed Fe-SMA), two specimens were tested. To pre-stress the specimens, they were stored in an oven and heated to 160 °C in less than two hours (thermal treatment). The influence of thermal treatment on the concrete's performance was found to be negligible. Due to the pre-stressing, the first crack loads increased from 12.0 to 31.9 kN, which indicates a growth of 166%. After cracks appeared in the specimens, the influence of the axial stiffness of the materials became clear. The greater EA and constant Young's modulus of the B500B resulted in stiffer force-strain curves and a nearly linear behavior in the fully cracked state. Compared to that, the nonactivated Fe-SMA rebars had softer behavior, and a decreasing Young's modulus at increasing stresses was observed. The loading curve of pre-stressed Fe-SMA rebar specimens proceeded nearly parallel to the inactivated ones after the cracking process ended. For the evaluation of the cracking process, a DIC measurement system was used. The crack spacings as well as the force-crack-opening curves differed for the tested specimens. While B500B had the smallest crack spacings and the steepest force-crack-opening curve, pre-stressing resulted in larger crack spacings. The bonding performance of the nonactivated and activated Fe-SMA specimens was found to be similar, which was shown via the converging force-crack-opening curves of both series.

6. Outlook

In practice, it is possible to anchor the Fe-SMA rebars only at the ends of the elements (i.e., cast in concrete) and activate pre-stressing in the free length (see Figure 2a). Afterwards, the pre-stressed rebars in the free length are then cast. In this case, the pre-stressing effect is transferred to the structural element at the ends, while the repair concrete is not pre-stressed. Thus, the system will probably result in reduced deflections and finer but earlier cracks. In further investigations, both methods (activation of the Fe-SMA embedded solely on the ends and pre-stressing the fully embedded Fe-SMA rebar; compare Figure 2a,b) will be analyzed and compared via bending tests. Furthermore, the DIC measurement system will be utilized to show the strain distribution on the specimen during the pre-stressing process.

Author Contributions: Investigation, M.B.; resources, C.C.; supervision, J.O.; writing—original draft, M.B. and J.O.; writing—review & editing, C.C. All authors have read and agreed to the published version of the manuscript.

Funding: This research received no external funding.

Institutional Review Board Statement: Not applicable.

Informed Consent Statement: Not applicable.

Data Availability Statement: The data presented in this study are available on request from the corresponding author. The data are not publicly available due to the presented results are pretest for a research project. The Data will be available publicly at the end of the research project.

Acknowledgments: We would like to thank Julien Michels (refer AG, Switzerland) for providing the iron-based shape memory alloys as well as helpful information and discussions.

Conflicts of Interest: The authors declare no conflict of interest.

References

1. Zheng, B.; Dawood, M. Fatigue Strengthening of Metallic Structures with a Thermally Activated Shape Memory Alloy Fiber-Reinforced Polymer Patch. *J. Compos. Constr.* **2017**, *21*, 4016113. [\[CrossRef\]](#)
2. Mas, B.; Cladera, A.; Ribas, C. Experimental study on concrete beams reinforced with pseudoelastic Ni-Ti continuous rectangular spiral reinforcement failing in shear. *Eng. Struct.* **2016**, *127*, 759–768. [\[CrossRef\]](#)
3. Debska, A.; Gwozdziwicz, P.; Seruga, A.; Balandraud, X.; Destrebecq, J.F. Prestress state evolution during thermal activation of memory effect in concrete beams strengthened with external SMA wires. *Arch. Civ. Mech. Eng.* **2020**, *20*, 142. [\[CrossRef\]](#)
4. Choi, E.; Cho, S.-C.; Hu, J.W.; Park, T.; Chung, Y.-S. Recovery and residual stress of SMA wires and applications for concrete structures. *Smart Mater. Struct.* **2010**, *19*, 94013. [\[CrossRef\]](#)
5. Tran, H.; Balandraud, X.; Destrebecq, J.F. Improvement of the mechanical performances of concrete cylinders confined actively or passively by means of SMA wires. *Arch. Civ. Mech. Eng.* **2015**, *15*, 292–299. [\[CrossRef\]](#)
6. Suhail, R.; Amato, G.; McCrum, D.P. Active and passive confinement of shape modified low strength concrete columns using SMA and FRP systems. *Compos. Struct.* **2020**, *251*, 112649. [\[CrossRef\]](#)
7. Normenausschuss Bauwesen (NABau) im DIN. *EN 1504—Products and Systems for the Protection and Repair of Concrete Structures—Definitions, Requirements, Quality Control and Evaluation of Conformity*; German Version; Beuth Verlag GmbH: Berlin, Germany, 2005.
8. Raupach, M.; Orlowsky, J. *Erhaltung von Betonbauwerken. Baustoffe und Ihre Eigenschaften*, 1st ed.; Vieweg+Teubner Verlag; GWV Fachverlage GmbH: Wiesbaden, Germany, 2008; ISBN 9783835101203.
9. Dimmig-Osburg, A. Innovations Based on PCC. *AMR* **2013**, *687*, 369–377. [\[CrossRef\]](#)
10. Orlowsky, J.; Raupach, M. Textile reinforced sprayed mortar for the repair of hydraulic engineering structures. In *Concrete Repair, Rehabilitation and Retrofitting III—Proceedings of the 3rd International Conference on Concrete Repair, Rehabilitation and Retrofitting, ICCRRR 2012, Cape Town, South Africa, 3–5 September 2012*; CRC Press: London, UK, 2012; pp. 1065–1070. ISBN 9780415899529.
11. Michels, J.; Shahverdi, M.; Czaderski, C.; El-Hacha, R. Mechanical Performance of Fe-SMA Ribbed Bars for Concrete Prestressing. *ACI Mater. J.* **2018**, *115*. [\[CrossRef\]](#)
12. Alfes, C.; Fingerloos, F.; Flohrer, C. Wesentliche Änderungen in der neuen DAfStb-WU-Richtlinie 2017. *Beton und Stahlbetonbau* **2018**, *113*, 11–19. [\[CrossRef\]](#)
13. Deutscher Ausschuss für Stahlbeton e.V. *DAfStb-Richtlinie—Wasserundurchlässige Bauwerke aus Beton (WU-Richtlinie)*; Beuth Verlag GmbH: Berlin, Germany, 2017.
14. Knab, F.; Weber, A.; Schweinfurth, J. Sicherer Einsatz von Glasfaserbewehrung im Bauwesen. *Beton und Stahlbetonbau* **2015**, *110*, 822–831. [\[CrossRef\]](#)
15. Curbach, M.; Ortlepp, R. (Eds.) *Textilbeton in Theorie und Praxis*. In *Proceedings of the Tagungsband zum 6. Kolloquium zu Textilbewehrten Tragwerken (CTRS6), Gemeinsames Abschlusskolloquium der Sonderforschungsbereiche 528 (Dresden) und 532 (Aachen), Berlin, Germany, 19–20 September 2011*; Technische Universität: Dresden, Germany, 2011; ISBN 9783867802451.
16. Weiland, S.; Schladitz, F.; Schütze, E.; Timmers, R.; Curbach, M. Rissinstandsetzung eines Zuckersilos. *Bautechnik* **2013**, *90*, 498–504. [\[CrossRef\]](#)
17. Jesse, F.; Curbach, M. Verstärken mit Textilbeton. In *2010 Beton-Kalender: Brücken—Betonbau im Wasser*, 99th ed.; Bergmeister, K., Fingerloos, F., Wörner, J.-D., Eds.; Ernst & Sohn Verlag: Berlin, Germany, 2010; pp. 457–565. ISBN 9783433600443.
18. Shahverdi, M.; Czaderski, C.; Annen, P.; Motavalli, M. Strengthening of RC beams by iron-based shape memory alloy bars embedded in a shotcrete layer. *Eng. Struct.* **2016**, *117*, 263–273. [\[CrossRef\]](#)
19. Schranz, B.; Czaderski, C.; Vogel, T.; Shahverdi, M. Bond behaviour of ribbed near-surface-mounted iron-based shape memory alloy bars with short bond lengths. *Mater. Des.* **2020**, *191*, 108647. [\[CrossRef\]](#)
20. Saiidi, M.S.; Wang, H. Exploratory Study of Seismic Response of Concrete Columns with Shape Memory Alloys Reinforcement. *ACI Struct. J.* **2006**, *103*, 436–443. [\[CrossRef\]](#)
21. Strieder, E.; Aigner, C.; Petautschnig, G.; Horn, S.; Marcon, M.; Schwenn, M.; Zeman, O.; Castillo, P.; Wan-Wendner, R.; Bergmeister, K. Strengthening of Reinforced Concrete Beams with Externally Mounted Sequentially Activated Iron-Based Shape Memory Alloys. *Materials* **2019**, *12*, 345. [\[CrossRef\]](#)
22. Cladera, A.; Weber, B.; Leinenbach, C.; Czaderski, C.; Shahverdi, M.; Motavalli, M. Iron-based shape memory alloys for civil engineering structures: An overview. *Constr. Build. Mater.* **2014**, *63*, 281–293. [\[CrossRef\]](#)
23. Janke, L. Applications of shape memory alloys in civil engineering structures—Overview, limits and new ideas. *Mater. Struct.* **2005**, *38*, 578–592. [\[CrossRef\]](#)
24. Lee, W.J.; Weber, B.; Feltrin, G.; Czaderski, C.; Motavalli, M.; Leinenbach, C. Phase transformation behavior under uniaxial deformation of an Fe–Mn–Si–Cr–Ni–VC shape memory alloy. *Mater. Sci. Eng. A* **2013**, *581*, 1–7. [\[CrossRef\]](#)
25. Dong, Z.; Klotz, U.E.; Leinenbach, C.; Bergamini, A.; Czaderski, C.; Motavalli, M. A Novel Fe–Mn–Si Shape Memory Alloy with Improved Shape Recovery Properties by VC Precipitation. *Adv. Eng. Mater.* **2009**, *11*, 40–44. [\[CrossRef\]](#)
26. Shahverdi, M.; Michels, J.; Czaderski, C.; Motavalli, M. Iron-based shape memory alloy strips for strengthening RC members: Material behavior and characterization. *Constr. Build. Mater.* **2018**, *173*, 586–599. [\[CrossRef\]](#)
27. Niendorf, T.; Brenne, F.; Krooß, P.; Vollmer, M.; Günther, J.; Schwarze, D.; Biermann, H. Microstructural Evolution and Functional Properties of Fe–Mn–Al–Ni Shape Memory Alloy Processed by Selective Laser Melting. *Metall. Mater. Trans. A* **2016**, *47*, 2569–2573. [\[CrossRef\]](#)

28. Vollmer, M.; Arold, T.; Kriegel, M.J.; Klemm, V.; Degener, S.; Freudenberger, J.; Niendorf, T. Promoting abnormal grain growth in Fe-based shape memory alloys through compositional adjustments. *Nat. Commun.* **2019**, *10*, 2337. [[CrossRef](#)] [[PubMed](#)]
29. Michels, J.; Shahverdi, M.; Czaderski, C. Flexural strengthening of structural concrete with iron-based shape memory alloy strips. *Struct. Concr.* **2018**, *19*, 876–891. [[CrossRef](#)]
30. re-fer AG. References. Available online: <https://www.re-fer.eu/en/references/> (accessed on 14 December 2020).
31. Deutsches Institut für Normung. *EN 1015-11 Methods of Test for Mortar for Masonry—Part 11: Determination of Flexural and Compressive Strength of Hardened Mortar*; German Version; Beuth Verlag GmbH: Berlin, Germany, 2020.
32. re-fer AG. Product Data Sheet: Re-Bar. Available online: <https://www.re-fer.eu/downloads/> (accessed on 23 November 2020).
33. Schranz, B.; Czaderski, C.; Michels, J.; Vogel, T.; Motavalli, M. Ribbed iron-based shape memory alloy bars for pre-stressed strengthening applications. In *IABSE Symposium 2019 Guimarães, towards a Resilient Built Environment Risk and Asset Management*; International Association for Bridge and Structural Engineering: Zürich, Switzerland, 2019; ISBN 9783857481635.
34. Normenausschuss Eisen und Stahl (FES) im DIN; Normenausschuss Bauwesen (NABau) im DIN. *DIN 488-1 Betonstahl—Teil 1: Stahlsorten, Eigenschaften, Kennzeichnung*; Normenausschuss Eisen und Stahl (FES) im DIN; Normenausschuss Bauwesen (NABau) im DIN: Berlin, Germany, 2009.
35. DIN German Institute for Standardization. *Eurocode 2: Design of Concrete Structures—Part 1-1: General Rules and Rules for Buildings*; German Version EN 1992-1-1:2004 + AC:2010; Beuth Verlag GmbH: Berlin, Germany, 2011.
36. Schranz, B.; Figueiredo Nunes, M.; Czaderski, C.; Shahverdi, M. Bond modelling of near-surface-mounted memory-steel bars for prestressing based on fiberoptic strain measurements. *Constr. Build. Mater.* **2020**. In Review.